Discrete approximations of acoustic source distributions

Discrete Approximations of Acoustic Source Distributions

Stefan Bilbao, *Senior Member, IEEE*

***Abstract*—The modeling of source distributions of finite spatial extent in ultrasound and medical imaging applications is a problem of longstanding interest. In time domain methods, such as the finite difference time domain or pseudospectral approaches, one requirement is the representation of such distributions over a grid, normally Cartesian. Various artefacts, including staircasing errors, can arise. In this short contribution, the problem of the representation of a distribution over a grid is framed as an optimisation problem in the Fourier domain over a preselected set of grid points, thus maintaining control over computational cost, and allowing the fine tuning of the optimisation to the wavenumber range of interest for a particular numerical method. Numerical results are presented in the important special case of the spherical cap or bowl source.**

***Index Terms*—finite difference time domain method, acoustic simulation, ultrasonic transducers.**

I. Introduction

TIME domain simulation of the acoustic field for applications in ultrasound and medical imaging has a long history; early approaches include the finite difference time domain (FDTD) method [1], [2], [3], and, more recently, pseudospectral and k-space methods have been employed [4], [5]. See [6] for an overview. For all such methods, a 3D Cartesian grid is employed, and a major problem is the representation of source distributions of finite spatial extent. Key issues are staircasing effects [7], [5], [8] as well as the computational cost associated with the number of grid points required to represent a distribution [9]. In some approaches, grid point distributions are determined directly through geometric considerations, with additional local scaling techniques, alongside other local constraints (such as simply-connectedness of distributions) [10], [7]. In others, the spatial convolution of the source distribution with a bandlimited kernel is employed [8].

In this short contribution, an alternative method of approximating a source distribution over a Cartesian grid is shown. Here, the entire distribution is used as the starting point for an optimisation carried out in the wave vector domain; in order to maintain control over computational cost, the number of grid points may be chosen a priori, with a best solution following from the specification of a wavenumber range, which may be tuned according to the particular numerical method employed. Source distributions and their Fourier transforms are introduced in Section II, and discrete approximations over a 3D grid, and Fourier-based optimisation techniques in Section III. Numerical results in the special case of the spherical cap or bowl source distribution appear in Section IV.

S. Bilbao is with the Acoustics and Audio Group, University of Edinburgh, Edinburgh, United Kingdom; e-mail: s.bilbao@ed.ac.uk.

II. Source Distributions

In the simplest case, the 3D wave equation is the target system to be solved numerically:

$$\frac{1}{c^2}\partial_t^2 p - \nabla^2 p = S(\mathbf{x}, t)\,. \tag{1}$$

Here $p(\mathbf{x}, t)$ is the pressure, as a function of $\mathbf{x} \in \mathbb{R}^3$ and $t \in \mathbb{R}$; here we consider an unbounded domain, so boundary conditions are not taken into account. We make here the further simplification [9] that the source term is separable as $S(\mathbf{x}, t) = g(\mathbf{x})f(t)$, for a fixed distribution $g(\mathbf{x})$ and driving function $f(t)$. Distributions are assumed normalised, so that

$$\iiint_{\mathbb{R}^3} g(\mathbf{x}) d\mathbf{x} = 1\,. \tag{2}$$

The Fourier transform $G(\mathbf{k})$ of $g(\mathbf{x})$ is defined by

$$G(\mathbf{k}) = \iiint_{\mathbb{R}^3} g(\mathbf{x}) e^{-i\mathbf{k}\cdot\mathbf{x}} d\mathbf{x} \tag{3}$$

in terms of the wave vector $\mathbf{k} = [k_x,\, k_y,\, k_z] \in \mathbb{R}^3$.

The spherical cap is of great importance in ultrasound transducer modeling. See Table I for the distribution and its transform. Here, $\delta(\cdot)$ is a Dirac delta function, J_0 is the zeroth order Bessel function of the first kind, and the box function $\sqcap(\zeta) = H(\zeta + 1) - H(\zeta - 1)$ is defined in terms of the Heaviside step function $H(\zeta)$.

TABLE I
Distribution $g(\mathbf{x})$ and transform $G(\mathbf{k})$ for a spherical cap of radius R and polar angle ϕ_0, aligned with the z axis. Here, $\mathbf{x} = [r\cos(\theta),\, r\sin(\theta),\, z]$ and $\mathbf{k} = [k_r\cos(\psi),\, k_r\sin(\psi),\, k_z]$.

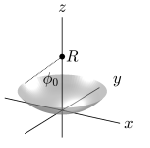

$$g(\mathbf{x}) = \frac{\delta\left(z - R + \sqrt{R^2 - r^2}\right) \sqcap\left(r/R\sin(\phi_0)\right)}{4\pi R \sin^2(\phi_0/2)\sqrt{R^2 - r^2}}$$

$$G(\mathbf{k}) = \int_{\cos(\phi_0)}^{1} \frac{e^{jk_z R(\eta-1)} J_0\left(Rk_r\sqrt{1-\eta^2}\right)}{2\sin^2(\phi_0/2)} d\eta$$

The Fourier transform of a rotated distribution $g_{\mathbf{R}}(\mathbf{x}) = g(\mathbf{R}\mathbf{x})$, for rotation matrix $\mathbf{R} \in SO(3)$ is $G_{\mathbf{R}}(\mathbf{k}) = G(\mathbf{R}\mathbf{k})$.

III. Discrete Approximations

Consider now approximation over a 3D grid, of spacing Δ_x, with grid points at $\mathbf{x} = \mathbf{q}\Delta_x$, $\mathbf{q} \in \mathbb{Z}^3$. See Figure 1. Two-step approximations to the wave equation (1) are of the form:

$$p_{\mathbf{q}}^{n+1} = 2p_{\mathbf{q}}^n - p_{\mathbf{q}}^{n-1} + c^2\Delta_t^2 \mathcal{L} p_{\mathbf{q}}^n + c^2\Delta_t^2 \tilde{g}_{\mathbf{q}} f^n\,. \tag{4}$$

Here, $p_{\mathbf{q}}^n$ is an approximation to $p(\mathbf{x} = \mathbf{q}\Delta_x, t = n\Delta_t)$, for integer time index n and time step Δ_t. $\mathcal{L}$ is a discrete approximation to the Laplacian, obtained either through local

difference operations, or through Fourier spectral discretisation (including possibly k-space scaling) [6]. f^n approximates $f(t)$, obtained, in the simplest case, through sampling.

An approximation $\tilde{g}_{\mathbf{q}}$ to the continuous distribution $g(\mathbf{x})$ is assumed defined over a region of finite support $\mathbf{q} \in \mathbb{D} \subset \mathbb{Z}^3$. The size of the set $\mathbb{D}$ will determine the computational cost of employing such an approximation in a simulation. The discrete Fourier transformation of $\tilde{g}_{\mathbf{q}}$ is $\tilde{G}(\mathbf{k})$, where

$$\tilde{G}(\mathbf{k}) = \Delta_x^3 \sum_{\mathbf{q}\in\mathbb{D}} \tilde{g}_{\mathbf{q}} e^{-i(\mathbf{k}\cdot\mathbf{q})\Delta_x} . \tag{5}$$

The factor Δ_x^3 is included for consistency with the continuous Fourier transform in (3). From basic sampling theory, the transform is assumed defined for wave vectors $\mathbf{k} \in \mathbb{U}_{\pi/\Delta_x}$, for the cube-shaped region $\mathbb{U}_{\pi/\Delta_x}$ defined by

$$\mathbb{U}_{\pi/\Delta_x} = \{\mathbf{k} \in \mathbb{R}^3 |\ \|\mathbf{k}\|_\infty \leq \pi/\Delta_x\} . \tag{6}$$

See Figure 1. In the present context, not all of this discrete range of wave vectors is useful; a Cartesian grid of spacing Δ_x cannot support isotropic wave propagation for wavenumbers $|\mathbf{k}| > \pi/\Delta_x$, regardless of the numerical method used. It is useful, for optimisation purposes, to introduce a bandlimited region in the wave vector domain, defined by $\mathbb{B}_\xi = \{\mathbf{k} \in \mathbb{R}^3 | |\mathbf{k}| \leq \xi\}$. Other non-Cartesian regular grid lattices can be used to increase spatial sampling efficiency [11], [12].

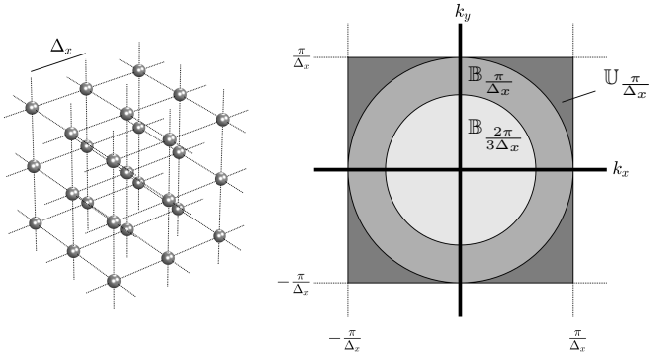

Fig. 1. Left: Cartesian grid, of spacing Δ_x. Right: planar cross section of the wave vector region $\mathbb{U}_{\pi/\Delta_x}$, showing spherical regions $\mathbb{B}_{\pi/\Delta_x}$ and $\mathbb{B}_{2\pi/3\Delta_x}$.

A. Optimisation

Given a target distribution $g(\mathbf{x})$, grid spacing Δ_x and a discrete domain $\mathbb{D}$, optimisation may be performed in the Fourier domain to yield an approximation $\tilde{g}_{\mathbf{q}}$. A simple approach is to optimise only over a wavenumber range $|\mathbf{k}| \leq \gamma\pi/\Delta_x$, for some γ with $0 < \gamma \leq 1$. The cost function is

$$E(g, \tilde{g}, \Delta_x, \mathbb{D}) = \iiint_{\mathbb{B}_{\gamma\pi/\Delta_x}} |G - \tilde{G}|^2 d\mathbf{k} \tag{7}$$

where $\tilde{G}$ may be written in terms of the coefficients $\tilde{g}_{\mathbf{q}}$ from (5). Here, wavenumbers $|\mathbf{k}| > \gamma\pi/\Delta_x$ are not considered, and thus large deviations in the optimised and target source distribution spectra may occur over this range.

A simple solution follows from the linear system

$$\mathbf{A}\tilde{\mathbf{g}} = \mathbf{b} . \tag{8}$$

Here, if the number of grid locations included in $\mathbb{D}$ is D, and the locations are ordered as $\mathbf{q}_1, \ldots, \mathbf{q}_D$, then $\tilde{\mathbf{g}} = [\tilde{g}_{\mathbf{q}_1}, \ldots, \tilde{g}_{\mathbf{q}_D}]^T$ is a length D column vector containing the optimal coefficients. The $D \times D$ matrix $\mathbf{A}$ has, for its (l, m)th entry, using the cost function from (7),

$$[\mathbf{A}]_{l,m} = \frac{\gamma^2 j_1 (\gamma\pi|\mathbf{q}_l - \mathbf{q}_m|)}{2|\mathbf{q}_l - \mathbf{q}_m|}, \tag{9}$$

where j_1 is the first order spherical Bessel function. Here, the condition number grows with the number of grid points (and also as the wavenumber range or γ decreases). For the cases illustrated in Section IV, D ranges from approximately 10^3 to 10^4, and a very small degree of regularisation (Tikhonov [13]) is sufficient to remove ill conditioning.

The $D \times 1$ column vector $\mathbf{b}$ has, for its lth entry

$$[\mathbf{b}]_l = \frac{1}{8\pi^3} \iiint_{\mathbb{B}_{\gamma\pi/\Delta_x}} G e^{i(\mathbf{k}\cdot\mathbf{q}_l)\Delta_x} d\mathbf{k} = (g * \beta)\,|_{\mathbf{x}=\mathbf{q}_l\Delta_x} . \tag{10}$$

Note that (10) reduces to the spatial convolution of the continuous distribution g with the spherically-bandlimited kernel $\beta(\mathbf{x}) = (\gamma^2/2|\mathbf{x}|\Delta_x^2) j_1 (\gamma\pi|\mathbf{x}|/\Delta_x)$, evaluated over the spatial locations $\mathbf{q}\Delta_x$ in the arbitrary domain $\mathbb{D}$. There is thus a link with convolution-based methods proposed in [8]. An advantage of optimisation over a natural spherical range of wave vectors is that, due to the simple behaviour of the Fourier transform under rotation (see Section II), for a rotation of a distribution using rotation matrix $\mathbf{R}$, $[\mathbf{b}]_l$ as defined in (10) above may be obtained easily using rotated grid locations $\mathbf{q}_{\mathbf{R},l} = \mathbf{R}\mathbf{q}_l$.

A weighting function could be employed (possibly including the wavenumber scaling used in the case of k-space methods). The parameter γ may be used to tune the optimisation according to the numerical dispersion characteristics (and thus the useful wavenumber range) of a particular scheme (e.g., $\gamma = 1$ for a dispersionless k-space method, and $\gamma < 1$ for a simpler FDTD scheme exhibiting dispersion). It could also be used to target a reduced wavenumber range including the driving frequency under continuous-wave (CW) excitation. The linear system in (8) may be complemented by additional constraints (such as, e.g., normalisation of $\tilde{\mathbf{g}}$, through $\Delta_x^3 \mathbf{1}^T \tilde{\mathbf{g}} = 1$, or other moment conditions [14], [15]), leading to a constrained optimisation problem [16].

IV. Numerical Results

All results here employ $c = 1500$ m·s^{-1}, $R = 20$ mm and $\phi_0 = \pi/6$ [9]. A first choice is that of the domain $\mathbb{D}$ used to represent the source distribution over a grid. A reasonable choice is to make use of grid points within a halo region of a specified thickness $H\Delta_x$ around the true source distribution. See Figure 2, illustrating the resulting coefficient sets under unrotated and rotated conditions and with $\gamma = 0.7$.

An eighth-order accurate (in time and space) compact two-step FDTD scheme of the diamond stencil variety (with maximal Courant number $1/\sqrt{3}$) is used here [17], [18]. In contrast with a k-space method, it exhibits numerical dispersion at low points-per-wavelength (PPW), although at a given PPW it is computationally less costly in the limit of large grid sizes.

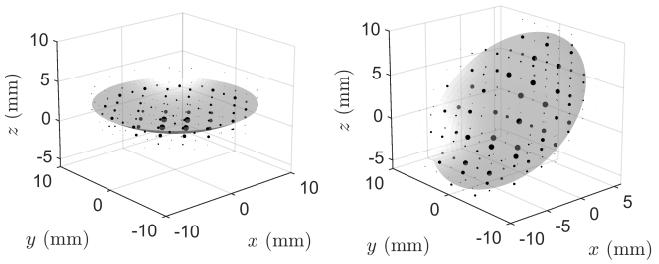

Fig. 2. Point clouds representing the spherical cap, unrotated (left) and rotated (right). Here, a halo thickness $H = 1$ grid points is used, with $\Delta_x = 2$ mm. Point sizes scale with the absolute size of the optimal coefficient.

See Figure 3. Pressure amplitudes due to CW excitation may be extracted through the Fourier transformation of an impulse response (i.e., using a Kronecker delta function for f in (1)).

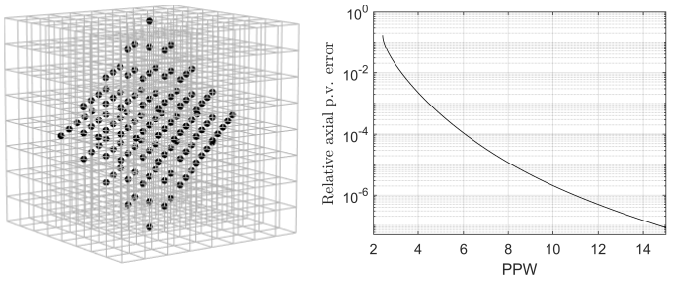

Fig. 3. Left: stencil for an eighth-order accurate FDTD scheme. Right: relative phase velocity error against PPW, in the (worst-case) axial propagation direction.

As a first example, the on-axis pressure amplitude for CW excitation generated by the scheme is compared with the approximate solution due to O'Neil [19]. See Figure 4, showing error for different PPW. Despite the dispersion error in the scheme, and the much smaller point cloud sizes relative to bandlimited interpolation methods used in k-space methods, the errors are comparable. Notice however, the slow convergence in the range near to the source plane—a feature consistent with other numerical results reported in the literature [7].

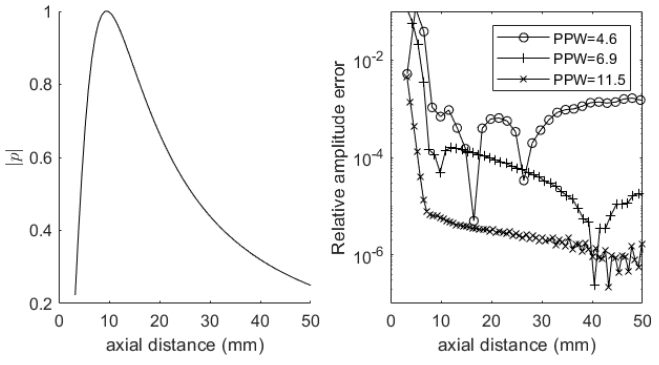

Fig. 4. Left: reference normalised on-axis pressure amplitude under CW conditions with an excitation frequency of 200 kHz. Right: relative on-axis absolute error, for different PPW, as indicated. Here, $\gamma = 0.35$ and $H = 4$.

In the previous example, the dispersion error of the scheme dominates over the error introduced by the approximation of the source term. To see more clearly the effects of the parameters γ and H, consider the case of operation at a high PPW, where the scheme dispersion is negligible. See Figure 5, illustrating axial pressure error under the variation of these parameters for a fixed sample rate. Notice in particular that even for very small point clouds ($H = 0.5$ corresponding to a halo region a single grid point thick), errors are on the order of 10^{-4}; for comparison, results using similar point cloud sizes obtained using heuristic scaling techniques [7] are also shown.

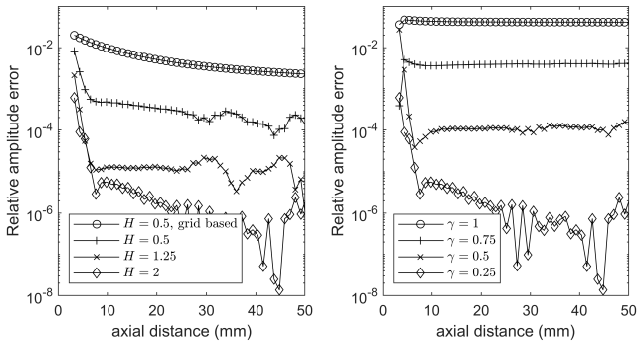

Fig. 5. Relative absolute error in the axial pressure amplitude, under variations in the thickness H in grid spacings Δ_x of the halo region, for fixed $\gamma = 0.25$ (left) and under variations in the relative bandwidth of the optimisation γ, for fixed $H = 2$ (right). In this case, CW excitation at 40 kHz is employed, and the sampling frequency is 2.4 MHz. Also shown, at left, are results for a simple grid-based source representation [7].

The procedure outlined above is insensitive to rotations of the source distribution. As an example, consider the bowl under two orientations: aligned with the z axis, and then rotated by $\pi/4$ about the y axis, as shown in Figure 2. As shown in Figure 6, there are no substantial differences in simulation errors between the two orientations.

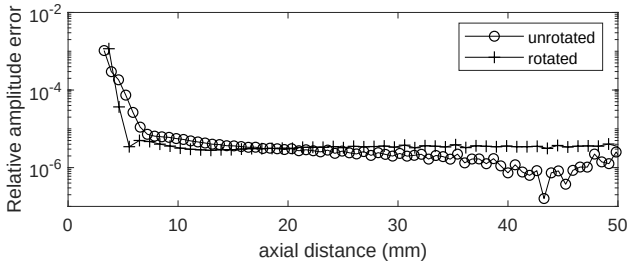

Fig. 6. On-axis error in pressure amplitude, under conditions as given in Figure 4, at 11.6 PPW, for unrotated and rotated bowl orientations.

V. Concluding Remarks

In this short contribution, a new approach to the representation of source distributions over a Cartesian grid has been illustrated. The key feature is the approximation of the distribution as a whole in the wave vector domain, and the reframing of the determination of a discrete representation as an optimisation problem. This allows for the sidestepping of staircasing problems, as well as control over eventual computational cost, and the ability to target particular wavenumber ranges. This approach is of general utility and is independent of the time stepping method used (e.g., FDTD or pseudospectral).

REFERENCES

[1] C. Manry and S. Broschat, "FDTD simulations for ultrasound propagation in a 2-D breast model," *Ultrasonic Imaging*, vol. 18, pp. 25–34, 1996.

[2] T. Mast, L. Hinkelman, M. Orr, V. Sparrow, and R. Waag, "Simulation of ultrasonic pulse propagation through the abdominal wall," *Journal of the Acoustical Society of America*, vol. 102, no. 2, pp. 1177–1190, 1997.

[3] I. Hallaj and R. Cleveland, "FDTD simulation of finite-amplitude pressure and temperature fields for biomedical ultrasound," *Journal of the Acoustical Society of America*, vol. 105, no. 5, pp. L7–L12, 1999.

[4] B. Treeby, B. Cox, and J. Jaros, "k-wave: A MATLAB toolbox for the time domain simulation of acoustic wave fields. User manual," 2016.

[5] J. Robertson, B. Cox, J. Jaros, and B. Treeby, "Accurate simulation of transcranial ultrasound propagation for ultrasonic neuromodulation and stimulation," *Journal of the Acoustical Society of America*, vol. 141, no. 3, pp. 1726–1738, 2017.

[6] M. Verweij, B. Treeby, K. van Dongen, and L. Demi, "Simulation of ultrasound fields," in *Comprehensive Biomedical Physics*, D. Panetta and M. Demi, Eds. Elsevier, 2014, pp. 465–500.

[7] E. Martin, Y. Ling, and B. Treeby, "Simulating focused ultrasound transducers using discrete sources on regular Cartesian grids," *IEEE Transactions on Ultrasonics Ferroelectrics and Frequency Control*, vol. 63, no. 10, pp. 1535–1542, 2016.

[8] E. Wise, B. Cox, and B. Treeby, "Staircase-free acoustic sources for grid-based models of wave propagation," in *IEEE International Ultrasonics Symposium*, Washington D.C., Sept. 2017.

[9] E. Wise, B. Cox, J. Jaros, and B. Treeby, "Representing arbitrary acoustic source and sensor distributions in Fourier collocation methods," *Journal of the Acoustical Society of America*, vol. 146, no. 1, pp. 278–288, 2019.

[10] Y. Ling, E. Martin, and B. Treeby, "A discrete source model for simulating bowl-shaped focused ultrasound transducers on regular grids: Design and experimental validation," in *IEEE International Ultrasonics Symposium*, Taipei, Taiwan, Oct. 2015.

[11] D. Petersen and D. Middleton, "Sampling and reconstruction of wave-number-limited functions in N-dimensional Euclidean spaces," *Information and Control*, vol. 5, pp. 279–323, 1962.

[12] B. Hamilton and S. Bilbao, "On finite difference schemes for the 3-d wave equation using non-cartesian grids," in *Proceedings of the Sound and Music Computing Conference*, Stockholm, Sweden, Aug. 2013, pp. 592–599.

[13] A. Tikhonov, "Solution of incorrectly formulated problems and the regularization method," *Soviet Math. Dokl.*, vol. 4, pp. 1035–1038, 1963.

[14] X. Yang, X. Zhang, Z. Li, and G. He, "A smoothing technique for discrete delta functions with application to immersed boundary method in moving boundary simulations," *Journal of Computational Physics*, vol. 228, pp. 7821–7836, 2009.

[15] B. Hosseini, N. Nigam, and J. Stockie, "On regularizations of the Dirac delta distribution," *Journal of Computational Physics*, vol. 305, pp. 423–447, 2016.

[16] S. Bilbao and B. Hamilton, "Directional sources in wave-based acoustic simulation," *IEEE/ACM Transactions on Audio Speech and Language Processing*, vol. 27, no. 2, pp. 415–428, 2019.

[17] J. Tuomela, "On the construction of arbitrary order schemes for the many dimensional wave equation," *BIT Numerical Mathematics*, vol. 36, no. 1, pp. 158–165, 1996.

[18] S. Bilbao and B. Hamilton, "Higher-order accurate two-step finite difference schemes for the many dimensional wave equation," *Journal of Computational Physics*, vol. 367, pp. 134–165, 2018.

[19] H. O'Neil, "Theory of focusing radiators," *Journal of the Acoustical Society of America*, vol. 21, no. 5, pp. 516–526, 1949.

Stefan Bilbao Stefan Bilbao (B.A. Physics, Harvard, 1992, MSc., PhD Electrical Engineering, Stanford, 1996 and 2001 respectively) is currently Professor of Acoustics and Audio Signal Processing in the Acoustics and Audio Group at the University of Edinburgh, and previously held positions at the Sonic Arts Research Centre, at the Queen's University Belfast, and the Stanford Space Telecommunications and Radioscience Laboratory. He is an Associate Editor of the IEEE/ACM Transactions on Audio Speech and Language Processing. He was born in Montreal, Quebec, Canada.